Relativistic Effects in Gamma-Ray Binary Systems

Dmitry Khangulyan
Rikkyo University (Tokyo)

Variable Galactic Gamma-Ray Sources III
May 4-6, 2015, Heidelberg

SED of LS5039

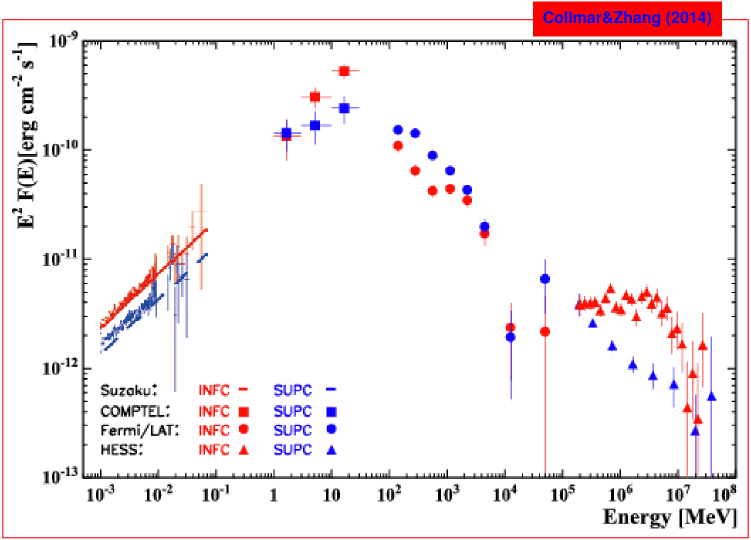

- Acceleration time if $E = \chi B$

$$t_{\mathrm{a}} = 0.1 \chi B_{\mathrm{G}}^{-1} E_{\mathrm{TeV}} \, \mathrm{s}$$

- Synchrotron Cooling

$$t_{\mathrm{syn}} = 400 B_{\mathrm{G}}^{-2} E_{\mathrm{TeV}}^{-1} \, \mathrm{s}$$

- Max. Electron Energy (in MHD setup: $\chi < 1$)

$$E_{\mathrm{max}} = 60 \eta^{-1/2} B_{\mathrm{G}}^{-1/2} \, \mathrm{TeV}$$

- Max. Synchrotron Energy

$$\hbar \omega_{\mathrm{max}} \sim 200 \chi^{-1} \, \mathrm{MeV}$$

SED of LS5039

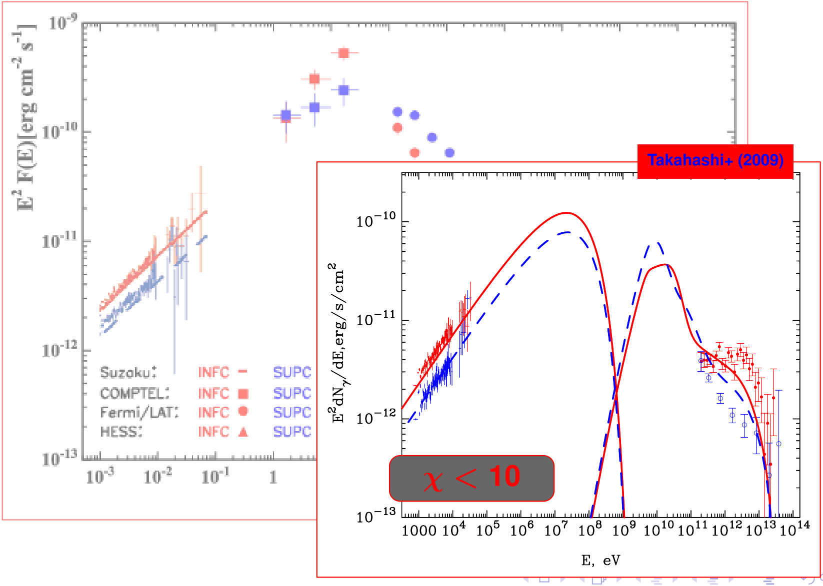

SED of LS5039

- Acceleration time if $E = \chi B$

$$t_{\rm a} = 0.1\chi B_{\rm G}^{-1} E_{\rm TeV}\ {\rm s}$$

- Synchrotron Cooling

$$t_{\rm syn} = 400 B_{\rm G}^{-2} E_{\rm TeV}^{-1}\ {\rm s}$$

- Max. Electron Energy (in MHD setup: $\chi < 1$)

$$E_{\rm max} = 60\chi^{-1/2} B_{\rm G}^{-1/2}\ {\rm TeV}$$

- Max. Synchrotron Energy

$$\hbar\omega_{\rm max} \sim 200\delta\chi^{-1}\ {\rm MeV}$$

$$\delta = (\Gamma(1-\beta\cos\theta))^{-1}$$

SED of LS5039

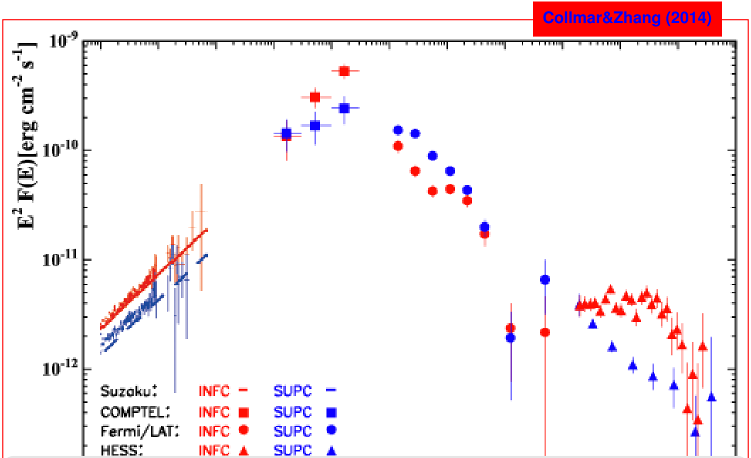

SED maximum at $30\mathrm{MeV}$ that *apparently* emerging from synchrotron X-ray spectra demands for a very efficient acceleration with $\chi < 10$. This requirement can be however relaxed if the emission is Doppler shifted.

GeV Flare from PSR B1259-63/LS2883

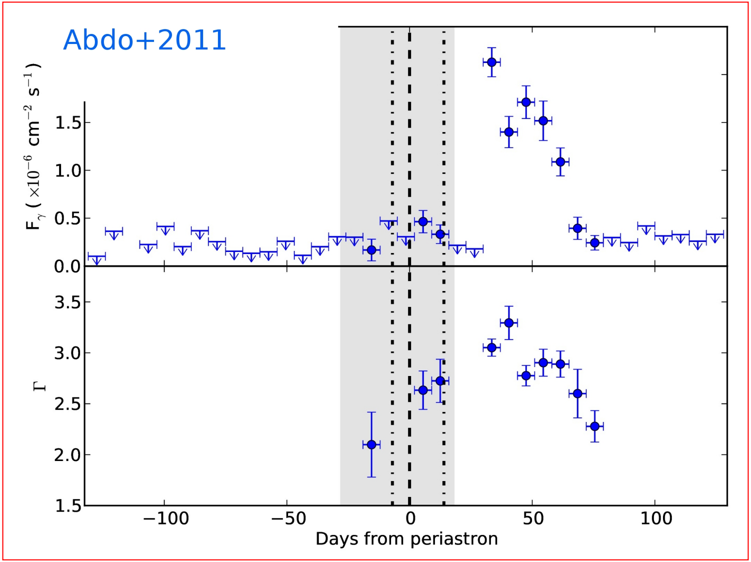

GeV Flare from PSR B1259-63/LS2883

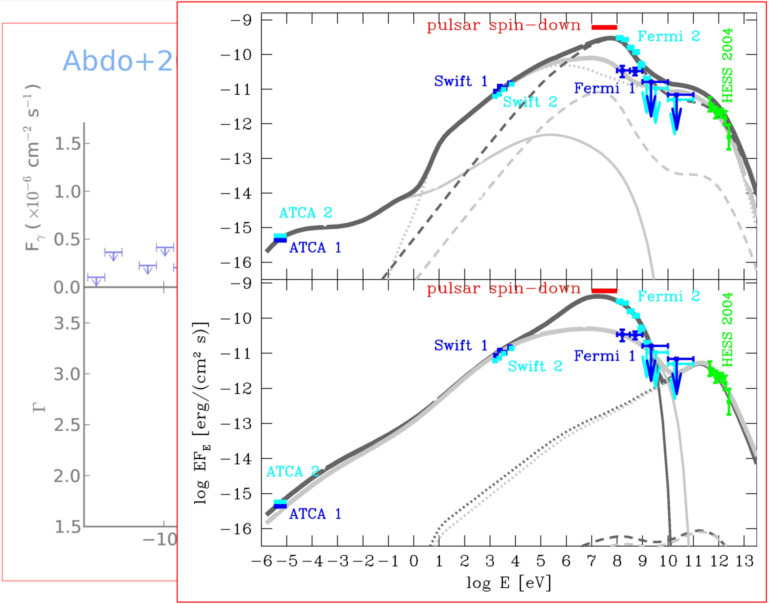

GeV Flare from PSR B1259-63/LS2883

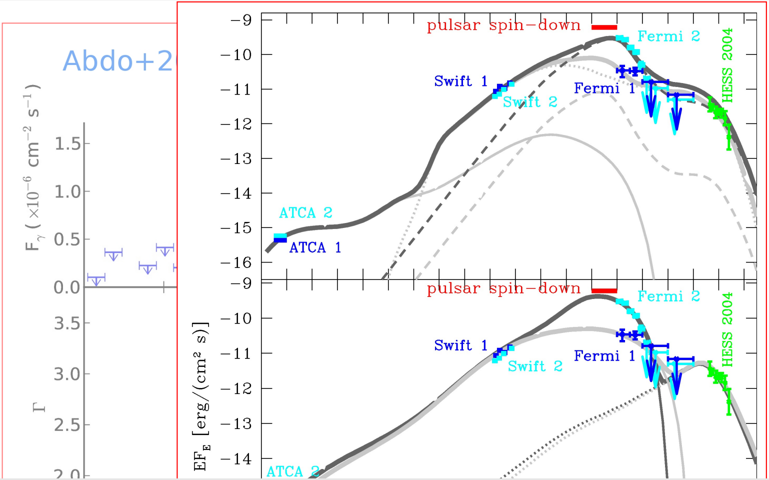

During the flare in PSR B1259-63/LS2883 the luminosity of the GeV component closely approached the spindown level. This requires unprecedentedly high conversion efficiency of pulsar rotation losses ⇒ non-thermal particles ⇒ to γ-rays.

GeV Flare from PSR B1259-63/LS2883

Credit: Pol,Victor,Carlo, Roman Krivonos

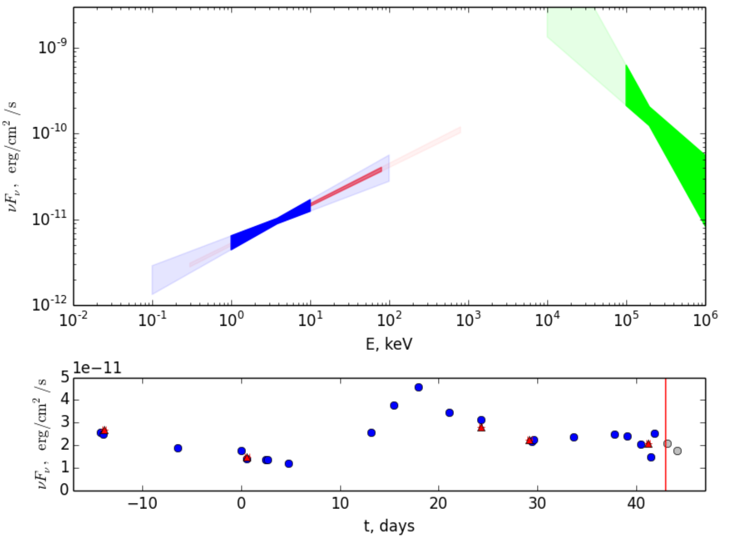

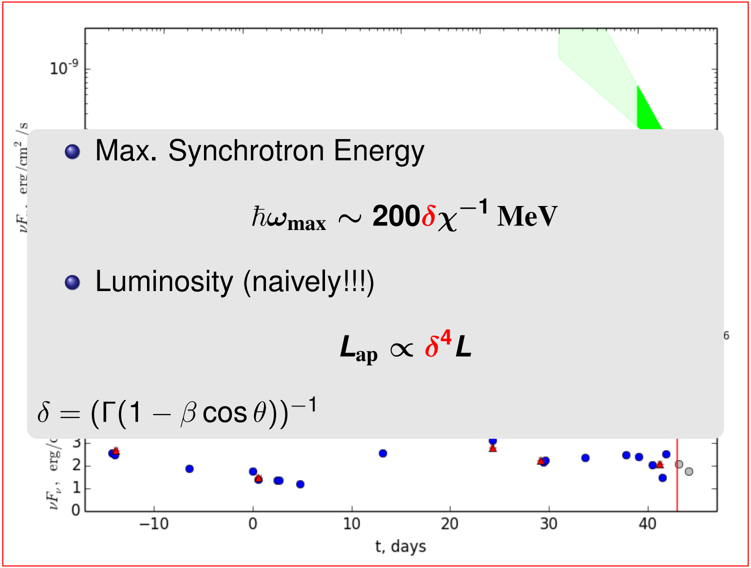

- Max. Synchrotron Energy

$$\hbar\omega_{\mathbf{max}} \sim 200\delta\chi^{-1}\,\mathbf{MeV}$$

- Luminosity (naively!!!)

$$L_{\mathbf{ap}} \propto \delta^4 L$$

$$\delta = (\Gamma(1-\beta\cos\theta))^{-1}$$

GeV Flare from PSR B1259-63/LS2883

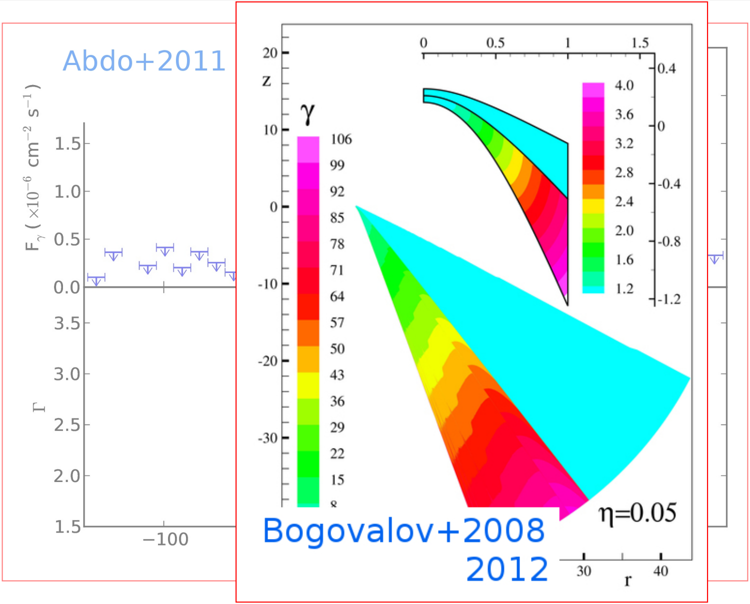

GeV Flare from PSR B1259-63/LS2883

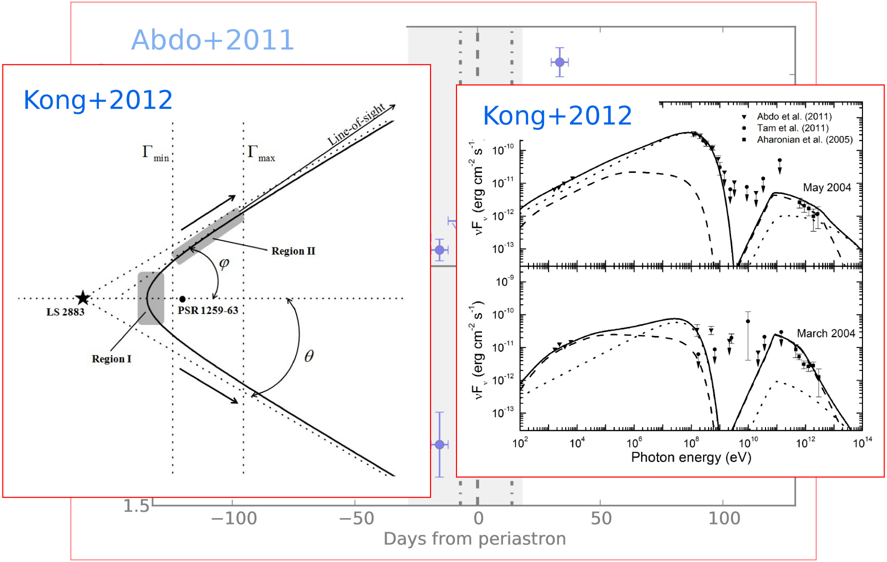

GeV Flare from PSR B1259-63/LS2883

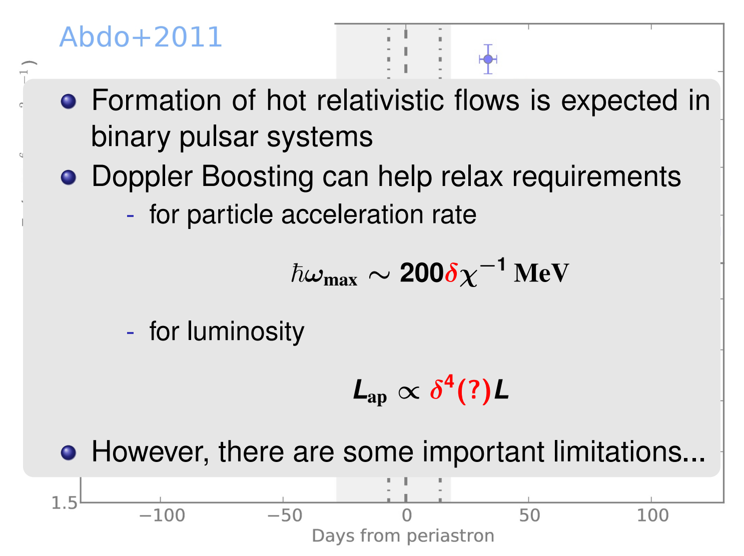

- Formation of hot relativistic flows is expected in binary pulsar systems
- Doppler Boosting can help relax requirements
  - for particle acceleration rate

$$\hbar\omega_{\mathrm{max}} \sim 200\delta\chi^{-1}\,\mathrm{MeV}$$

  - for luminosity

$$L_{\mathrm{ap}} \propto \delta^{4}(?)L$$

- However, there are some important limitations...

Hydrodynamics of wind interaction

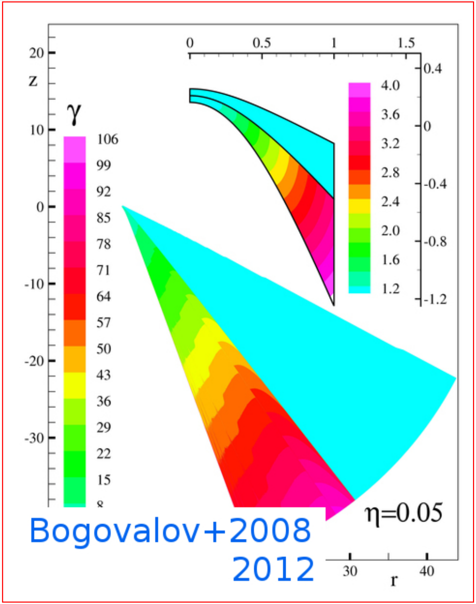

Hydrodynamics of wind interaction

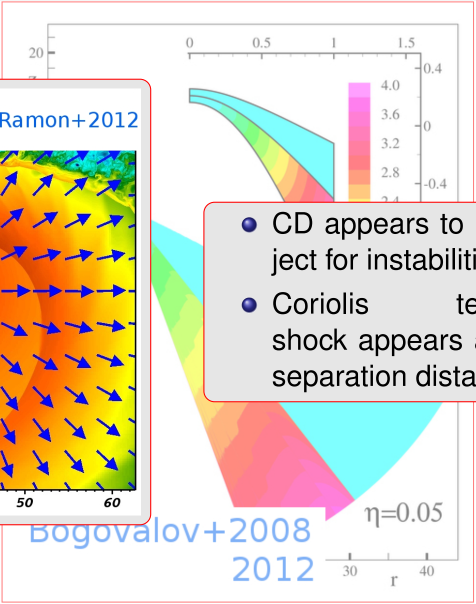

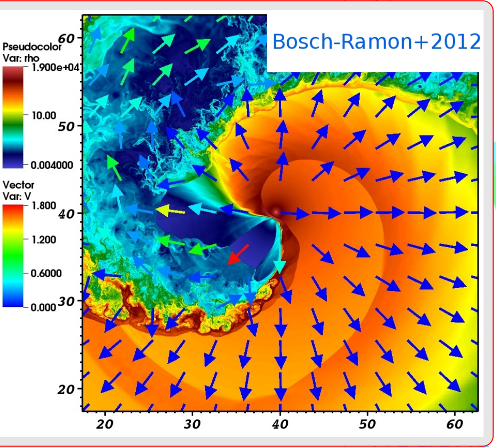

- CD appears to be a subject for instabilities
- Coriolis termination shock appears at several separation distances

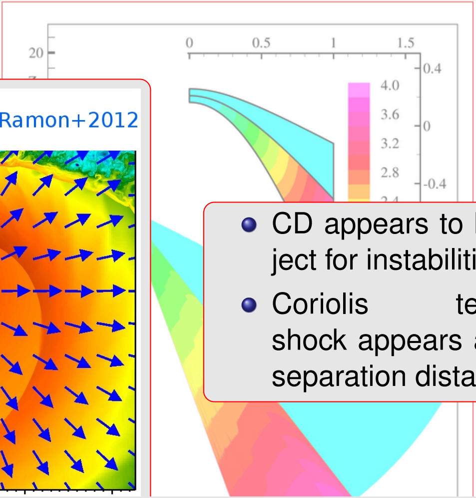

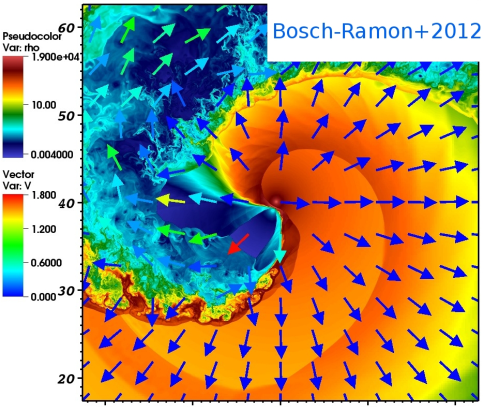

- CD appears to be a subject for instabilities
- Coriolis termination shock appears at several separation distances

However, perturbations significantly grow at several separation distances, but the structures in the inner part are consistent: cone-like outflow with plasma re-acceleration to relativistic velocities.

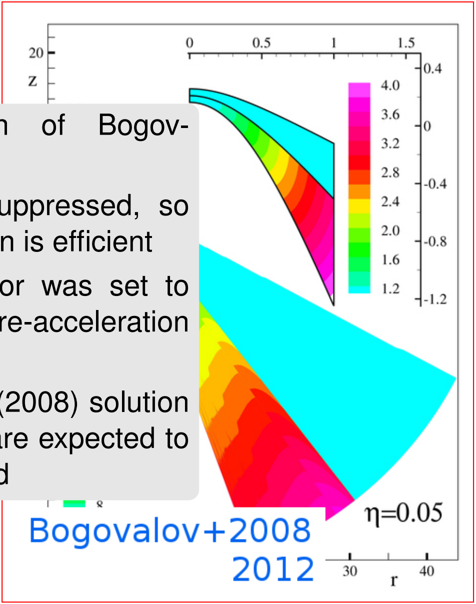

In the HD solution of Bogovalov+(2008)

- Instabilities are suppressed, so flow re-acceleration is efficient
- Wind Lorenz factor was set to $\Gamma_0 = 10^6$, so the re-acceleration is the fastest

So for the Bogovalov+(2008) solution the relativistic effects are expected to be strongly pronounced

Non-Thermal Emission in Shocked Pulsar Wind

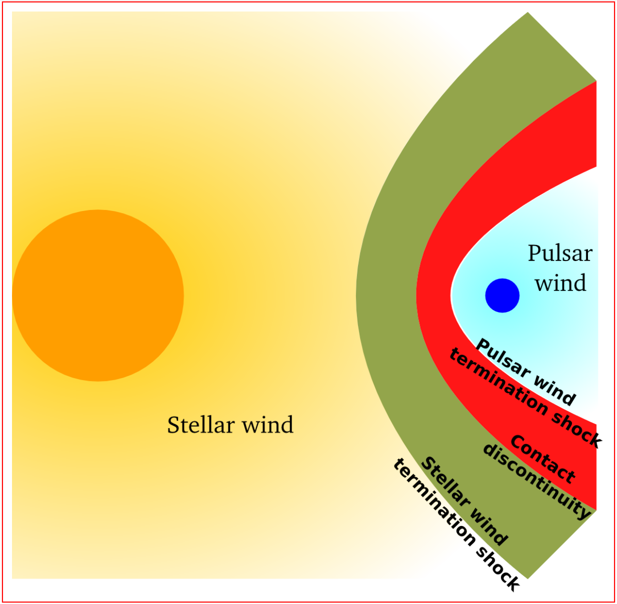

Non-Thermal Emission in Shocked Pulsar Wind

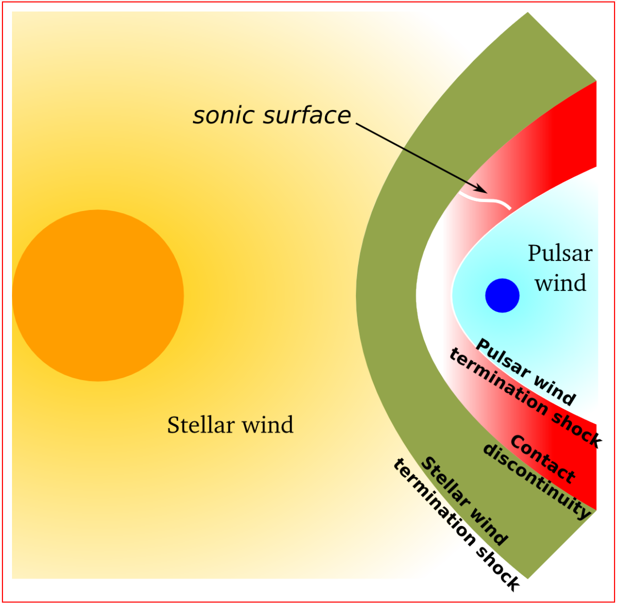

Non-Thermal Emission in Shocked Pulsar Wind

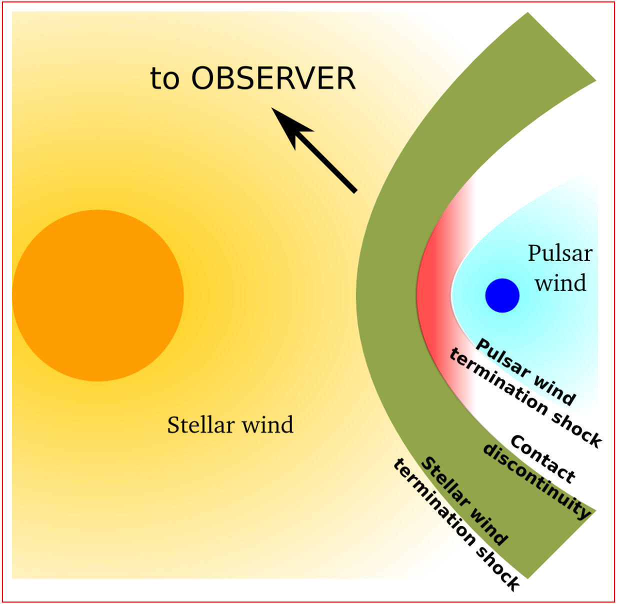

Non-Thermal Emission in Shocked Pulsar Wind

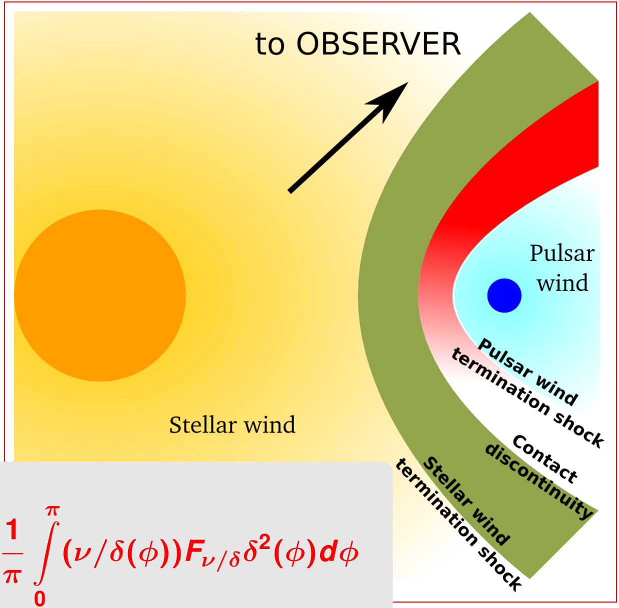

$$\nu F_{\nu,\mathrm{ap}} = \frac{1}{\pi}\int\limits_0^{\pi} (\nu/\delta(\phi)) F_{\nu/\delta}\delta^2(\phi)d\phi$$

Non-Thermal Emission in Shocked Pulsar Wind

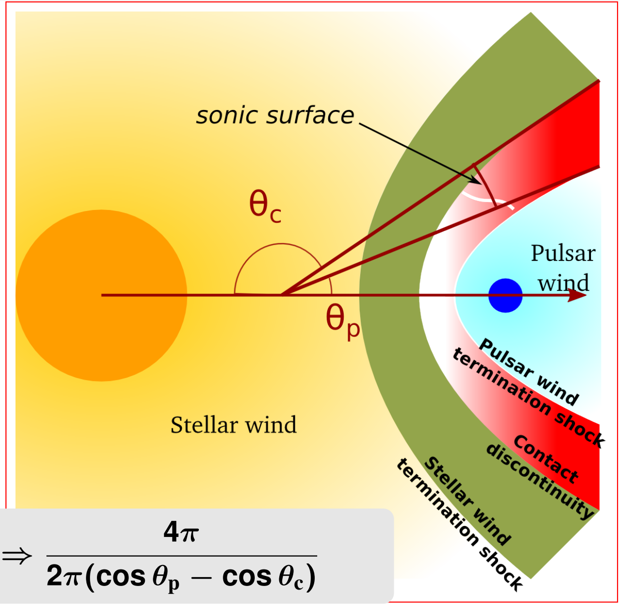

$$\delta(\phi)^2 \Rightarrow \frac{4\pi}{2\pi(\cos\theta_{\rm p} - \cos\theta_{\rm c})}$$

Non-Thermal Emission in Shocked Pulsar Wind

Bogovalov+(2008)

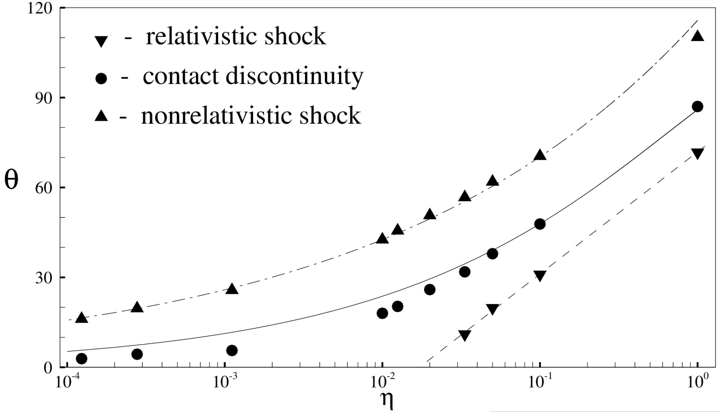

$$\theta_\mathrm{p} \simeq 41 \log \eta + 72$$
$$\theta_\mathrm{c} \simeq 29(4 - \eta^{0.4})\eta^{0.33}$$

Non-Thermal Emission in Shocked Pulsar Wind

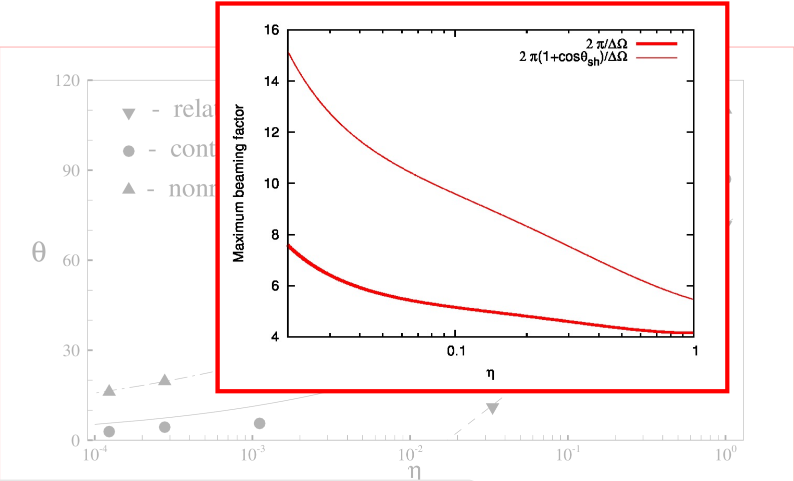

$$\delta(\phi)^2 \Rightarrow \frac{4\pi}{2\pi(\cos\theta_{\rm p} - \cos\theta_{\rm c})}$$

$$\theta_{\rm p} \simeq 41 \log\eta + 72$$
$$\theta_{\rm c} \simeq 29(4-\eta^{0.4})\eta^{0.33}$$

Non-Thermal Emission in Shocked Pulsar Wind

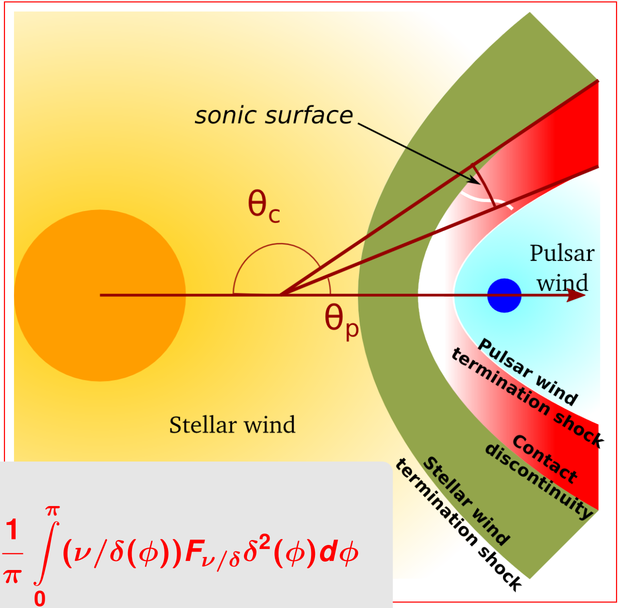

$$\nu F_{\nu,\mathrm{ap}} = \frac{1}{\pi}\int\limits_0^{\pi}(\nu/\delta(\phi))F_{\nu/\delta}\delta^2(\phi)d\phi$$

Non-Thermal Emission in Shocked Pulsar Wind

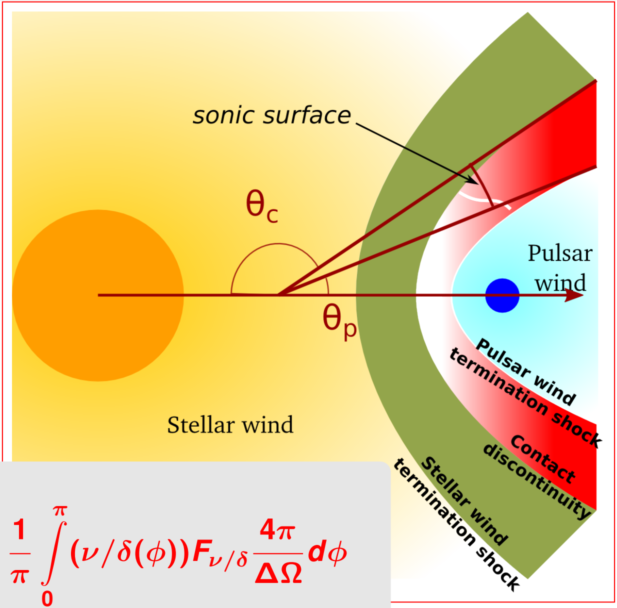

$$\nu F_{\nu,\mathrm{ap}} = \frac{1}{\pi}\int\limits_0^\pi (\nu/\delta(\phi)) F_{\nu/\delta} \frac{4\pi}{\Delta\Omega} d\phi$$

Non-Thermal Emission in Shocked Pulsar Wind

- Bernoulli Integral:

$$\frac{\Gamma w}{n} = \mathrm{const}$$

  for relativistic EOS: $\Gamma e = \mathrm{const}$, where e is specific internal energy

- Synchrotron characteristic energy: $\hbar\omega_{\mathrm{ap}} \propto \delta B E^2 \propto \Gamma^{-2}$
  - $\delta < 2\Gamma$
  - $E < E_0/\Gamma$
  - $B < B_0/\Gamma$

$$\nu F_{\nu,\mathrm{ap}} = \frac{1}{\pi}\int_0^{\pi} (\nu/\delta(\phi)) F_{\nu/\delta} \frac{4\pi}{\Delta\Omega} d\phi$$

Hydrodynamic Solution (Bogovalov+ 2008)

- Collision of non-relativistic stellar wind and relativistic pulsar wind
- Winds are spherical
- Hydrodynamic structure is determined by parameter $\eta = \frac{L_{\rm pulsar}}{\dot{M}_* V_{\rm wind} c}$
- Further assumptions:
  - To reduce instabilities at CD $V_{\rm wind} = c$ (but non-realistic equations for the stellar wind)
  - Pulsar wind velocity was assumed ultrarelativistic: $\Gamma_0 = 10^6$
  - Broad range of η-parameters has been studied: $10^{-4} < \eta < 1$

Hydrodynamic Solution (Bogovalov+ 2008)

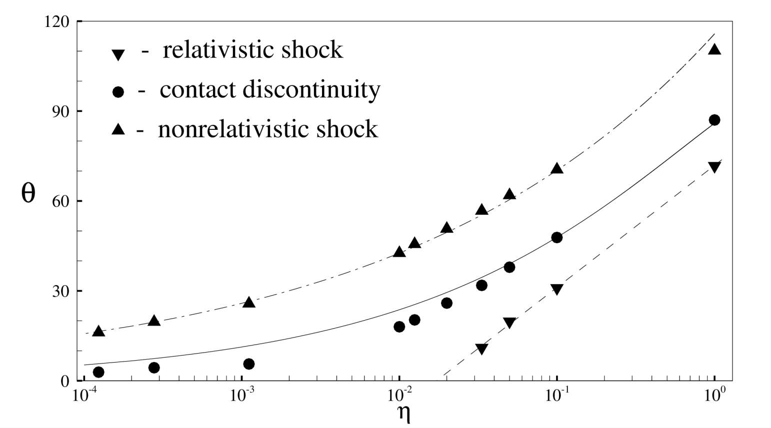

Hydrodynamic Solution (Bogovalov+ 2008)

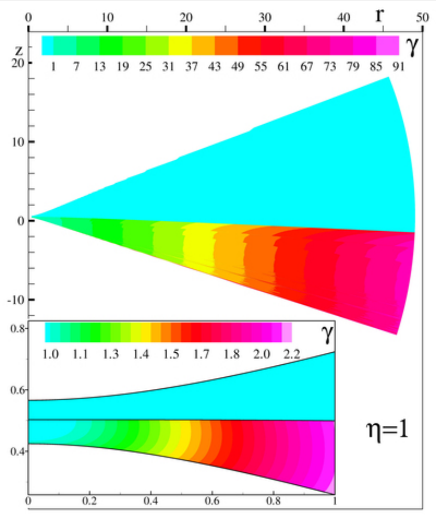

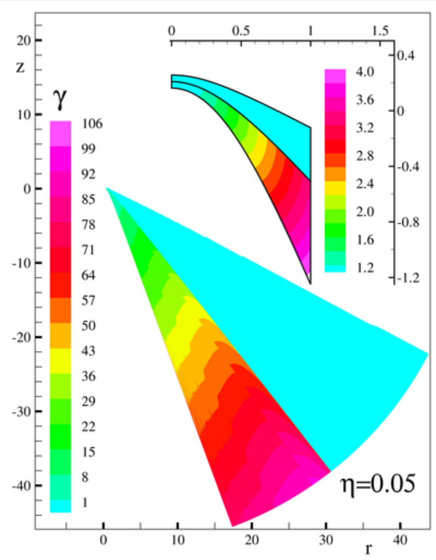

Hydrodynamic Solution (Bogovalov+ 2008)

- $\eta = 1$
- Number of current lines: $N_c = 1540$
- Number of points: $N_p > 3 \times 10^5$

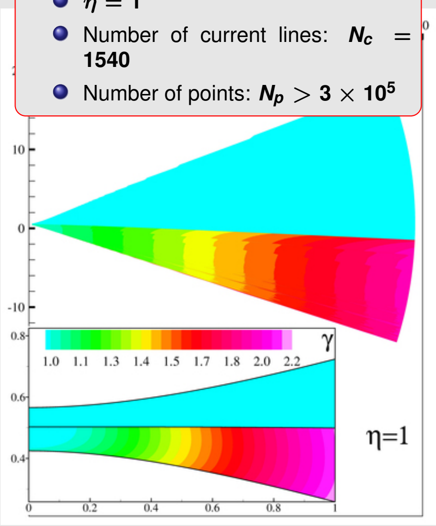

- $\eta = 0.05$
- Number of current lines: $N_c = 1680$
- Number of points: $N_p > 4 \times 10^5$

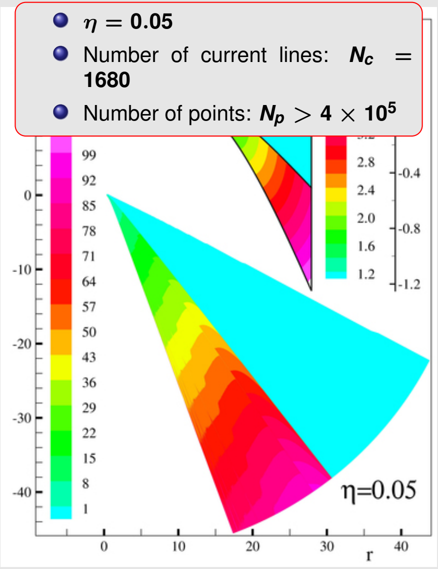

Hydrodynamic Solution: $\eta = 1$

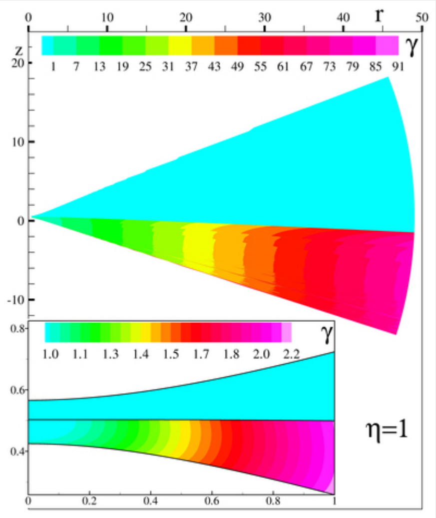

Hydrodynamic Solution:$\eta = 1$

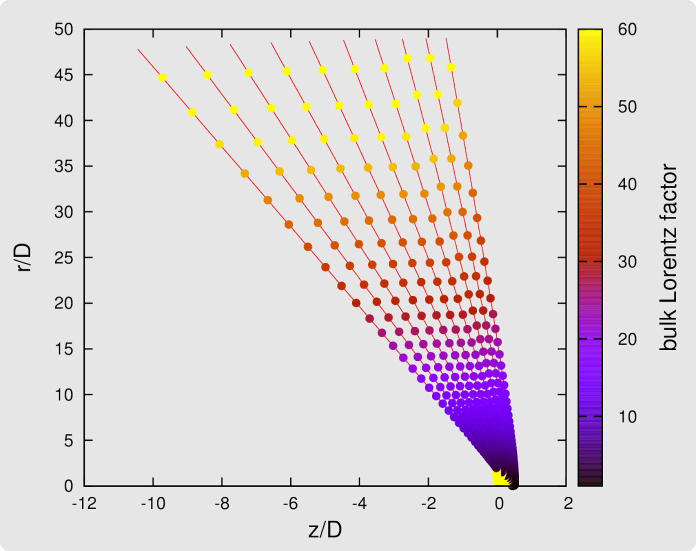

Hydrodynamic Solution: $\eta = 1$

- $\eta = 1$
- Number of current lines: $N_c = 1540$
- Number of points: $N_p > 3 \times 10^5$
- Treatment of non-thermal particles that accounts for
  - Particles acceleration at PW termination shock (phenomenological)
  - Advection with HD flow
  - Interaction with local magnetic field
  - Adiabatic cooling/heating
  - Interaction with local photon fields (accounting for photon dilution, aberration)
  - NOT accounting for the influence of radiative cooling on HD flow
  - NOT accounting for particle diffusion
- Code paralized with OpenMP

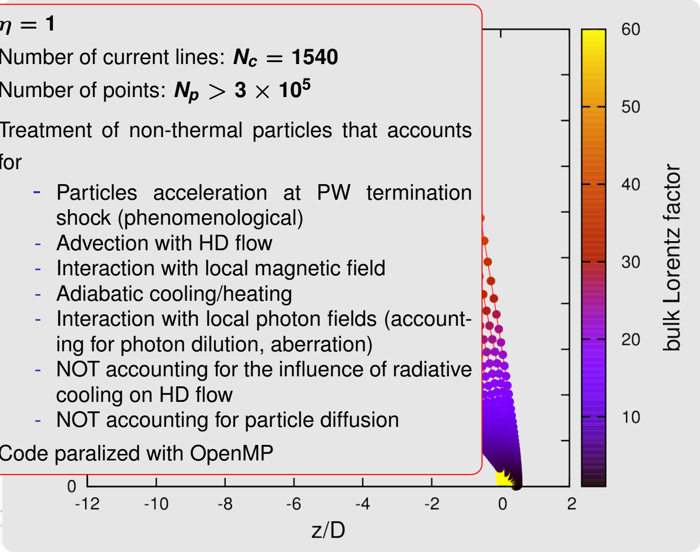

Hydrodynamic Solution: $\eta = 1$

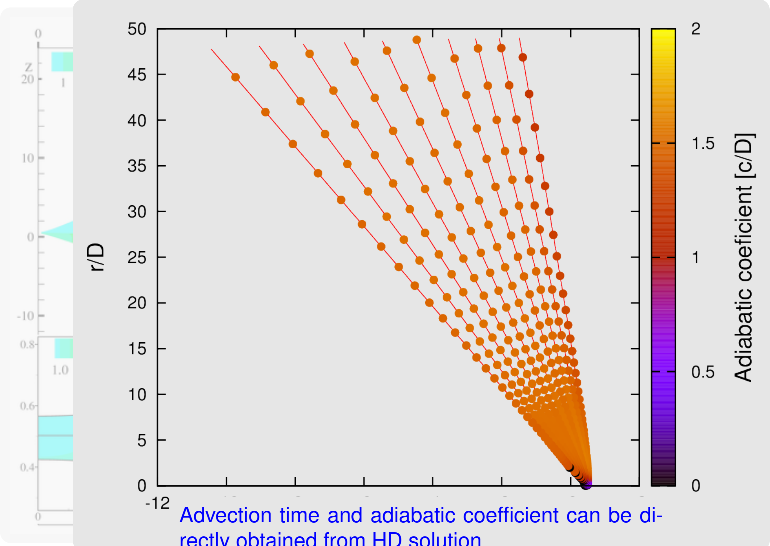

Advection time and adiabatic coefficient can be directly obtained from HD solution

Hydrodynamic Solution: $\eta = 1$

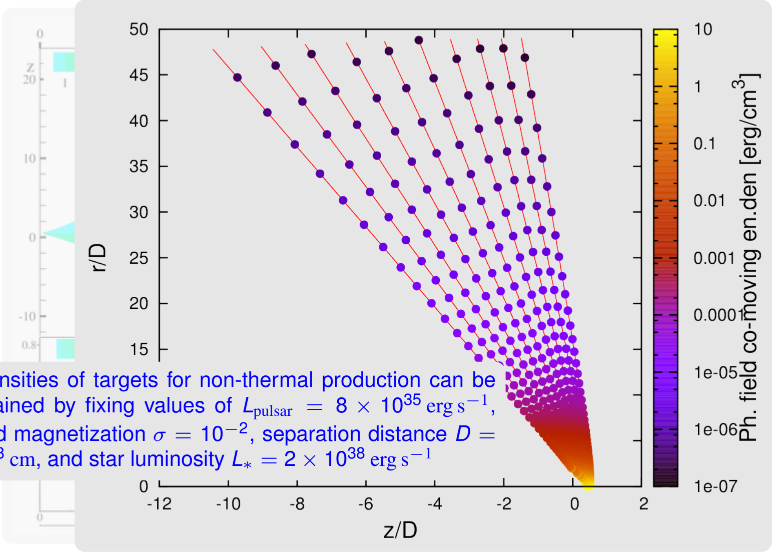

Intensities of targets for non-thermal production can be obtained by fixing values of $L_{\rm pulsar} = 8\times10^{35}\,{\rm erg\,s^{-1}}$, wind magnetization $\sigma = 10^{-2}$, separation distance $D = 10^{13}\,{\rm cm}$, and star luminosity $L_* = 2\times10^{38}\,{\rm erg\,s^{-1}}$

Treatment of IC losses and scattering

- Inverse Compton losses are to be computed in the co-moving frame, i.e., in a Planckian type photon field with modified temperature: $T_{\rm local} = \mathcal{D}_* T_*$, where $\mathcal{D}_* = \left[\Gamma\left(1 - (v_0/c)\cos\chi\right)\right]^{-1}$ (e.g., Khangulyan+2014)
- Inverse Compton emission should account for anisotropic scattering (Aharonian&Atoyan 1981, Bogovalov&Aharonian 2001) (this effectively implies a 3D computation of the IC emission even if the HD solution is 2D)

So, treatment of Inverse Compton process is very computationally expensive in this type of calculations, but if the dominant target is black-body type,

Treatment of IC losses and scattering

- IC scattering on BB:

$$\frac{dN_{\mathrm{ani/iso}}}{d\omega\, dt} = \frac{T^3 m_e^3 c^3 \kappa}{\pi^2 \hbar^3} \int\limits_{\epsilon_{\mathrm{ani/iso}}/T}^{\infty} \frac{d\nu_{\mathrm{ani/iso}}}{d\omega\, dN_{\mathrm{ph}}\, dt} \frac{x^2 dx}{\mathrm{e}^x - 1}\,.$$

- Approximate treatment as in Khangulyan+2014 (also Zdziarsky&Pjanka2014)

$$\frac{dN_{\mathrm{ani/iso}}}{d\omega\, dt} = \frac{2 r_o^2 m_e^3 c^4 \kappa T^2}{\pi \hbar^3 E^2} \times \left[\frac{z^2}{2(1-z)} F_1(x_0) + F_2(x_0)\right]$$

where $x_0 = \frac{z}{2(1-z)\, E_e T (1-\cos\theta) t_\theta}$, $z = E_\gamma / E_e$, and $F_{1,2}$ are simple functions of 1 argument

Treatment of IC losses and scattering

- IC scattering on BB:

$$\frac{dN_{\mathrm{ani/iso}}}{d\omega\, dt} = \frac{T^3 m_e^3 c^3 \kappa}{\pi^2 \hbar^3} \int\limits_{\epsilon_{\mathrm{ani/iso}}/T}^{\infty} \frac{d\nu_{\mathrm{ani/iso}}}{d\omega\, dN_{\mathrm{ph}}\, dt} \frac{x^2 dx}{e^x - 1} \,.$$

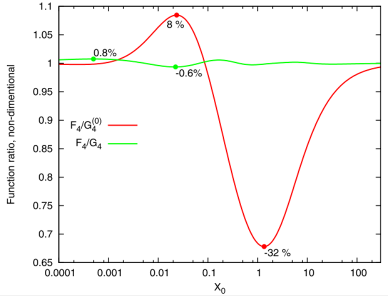

as

-2

— ×

—cos θ)

ument

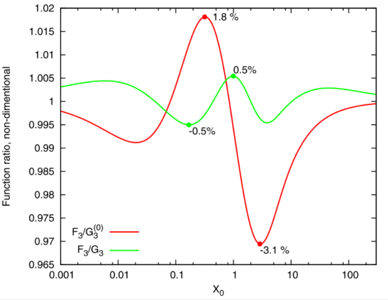

Treatment of IC losses and scattering

Representation of spectra										
F_1	Equation (11)	$G_1^{(0)} = \left(\frac{\pi^2}{6} + x_0\right) e^{-x_0}$	$\frac{z}{1-z}\frac{1}{2ET(1-\cos\theta)}$	…	…	…	…	…	∼10%	Figures 1 and 2
F_1	Equation (11)	$G_1^{(0)}(x_0) \times g(x_0)$	$\frac{z}{1-z}\frac{1}{2ET(1-\cos\theta)}$	0.153	0.857	0.254	1.84	…	<1%	Figures 1 and 2
F_2	Equation (11)	$G_2^{(0)} = \left(\frac{\pi^2}{6} + x_0\right) e^{-x_0}$	$\frac{z}{1-z}\frac{1}{2ET(1-\cos\theta)}$	…	…	…	…	…	∼50%	Figures 1 and 3
F_2	Equation (11)	$G_2^{(0)}(x_0) \times g(x_0)$	$\frac{z}{1-z}\frac{1}{2ET(1-\cos\theta)}$	1.33	0.691	0.534	1.668	…	<1%	Figures 1 and 3
F_3	Equation (14)	$G_3^{(0)} = \frac{\pi^2}{6}\frac{1+cx_0}{1+\frac{\pi^2 c}{6}x_0} e^{-x_0}$	$\frac{z}{1-z}\frac{1}{4ET}$	…	…	…	…	2.73	∼3%	Figures 4 and 5
F_3	Equation (14)	$G_3^{(0)}(x_0) \times g(x_0)$	$\frac{z}{1-z}\frac{1}{4ET}$	0.443	0.606	0.54	1.481	0.319	<1%	Figures 4 and 5
F_4	Equation (14)	$G_4^{(0)} = \frac{\pi^2}{6}\frac{1+cx_0}{1+\frac{\pi^2 c}{6}x_0} e^{-x_0}$	$\frac{z}{1-z}\frac{1}{4ET}$	…	…	…	…	47.1	∼30%	Figures 4 and 6
F_4	Equation (14)	$G_4^{(0)}(x_0) \times g(x_0)$	$\frac{z}{1-z}\frac{1}{4ET}$	0.726	0.461	0.382	1.457	6.62	<1%	Figures 4 and 6
Energy losses										
$F_{\rm ani}$	Equations (33) and (55)	$G_{\rm ani}^{(0)} = \frac{cu\log(1+2.16u/c)}{1+cu/0.822}$	$2ET(1-\cos\theta)$	…	…	…	—	6.13	∼1%	Figure 7
$F_{\rm iso}$	Equations (36) and (57)	$G_{\rm iso}^{(0)} = \frac{cu\log(1+0.722u/c)}{1+cu/0.822}$	$4ET$	…	…	…	—	4.62	∼5%	Figure 7
$F_{\rm iso}$	Equation (36)	$G_{\rm iso}^{(0)}(u) \times g(u)$	$4ET$	−0.362	0.682	0.826	1.281	5.68	∼1%	Figure 7
Interaction rate										
$F_{\rm n,ani}$	Equations (46) and (55)	$G_{\rm n,ani}^{(0)} = 0.822\log(1+1.949u)$	$2ET(1-\cos\theta)$	…	…	…	…	…	∼25%	Figure 8
$F_{\rm n,ani}$	Equation (46)	$G_{\rm n,ani}^{(0)}(u) \times g(u)$	$2ET(1-\cos\theta)$	1.05	0.885	2.46	1.213	…	∼1%	Figure 8
$F_{\rm n,iso}$	Equations (50) and (57)	$G_{\rm n,iso}^{(0)} = 0.822\log(1+0.97u)$	$4ET$	…	…	…	…	…	∼30%	Figure 8
$F_{\rm n,iso}$	Equation (50)	$G_{\rm n,iso}^{(0)}(u) \times g(u)$	$4ET$	0.829	0.88	1.27	1.135	…	∼1%	Figure 8
Mean energy of emitted photons										
$\bar z_{\rm ani}$	Equation (55)	$G_{\rm ani}^{(0)}/G_{\rm n,ani}^{(0)}$	$2ET(1-\cos\theta)$	…	…	…	—	4.26	∼3%	Figure 9
$\bar z_{\rm ani}$	Equation (56)	$\frac{u}{u+0.2}\frac{\log(1+u/2)}{\log(1+2u)}$	$2ET(1-\cos\theta)$	…	…	…	—	…	∼8%	Figure 9
$\bar z_{\rm iso}$	Equation (57)	$G_{\rm iso}^{(0)}/G_{\rm n,iso}^{(0)}$	$4ET$	…	…	…	—	2.9	∼5%	Figure 9
$\bar z_{\rm iso}$	Equation (58)	$\frac{u}{u+0.3}\frac{\log(1+u/4)}{\log(1+u)}$	$4ET$	…	…	…	—	…	∼8%	Figure 9
Energy of emitting particle										
t_θ	Equation (59)	$\frac{v^{1/2}(1+2v^{1/2})}{2}\sqrt{\frac{\log(1+v^{1/2})}{\log(1+v^{1/2}/3)}}$	$2\bar\omega T(1-\cos\theta)$	…	…	…	—	…	∼10%	…
t	Equation (59)	$\frac{v^{1/2}\left(1+2v^{1/2}\right)}{2}\sqrt{\frac{\log(1+v^{1/2})}{\log(1+v^{1/2}/4)}}$	$4\bar\omega T$	…	…	…	—	…	∼10%	…

So,
tior
nar

Emission from inner fluid lines

Emission by the most inner fluid line

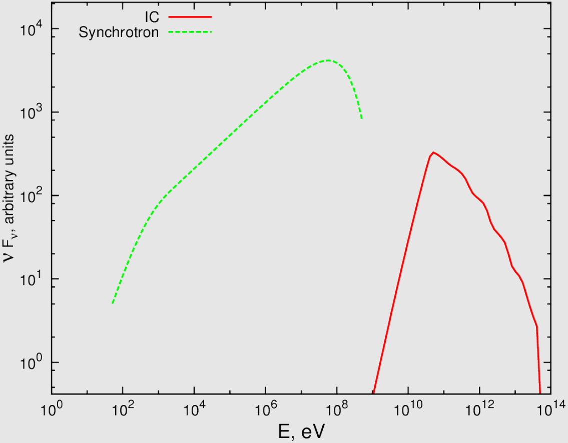

Emission from inner fluid lines

Emission by the 3 most inner fluid line

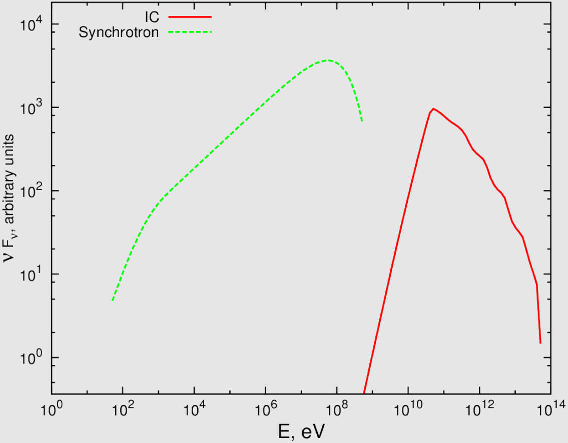

Emission from inner fluid lines

Emission by the 10 most inner fluid line

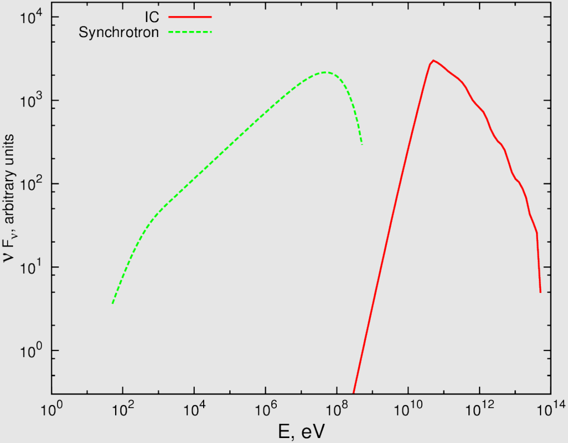

Hydrodynamic Solution: $\eta = 1$

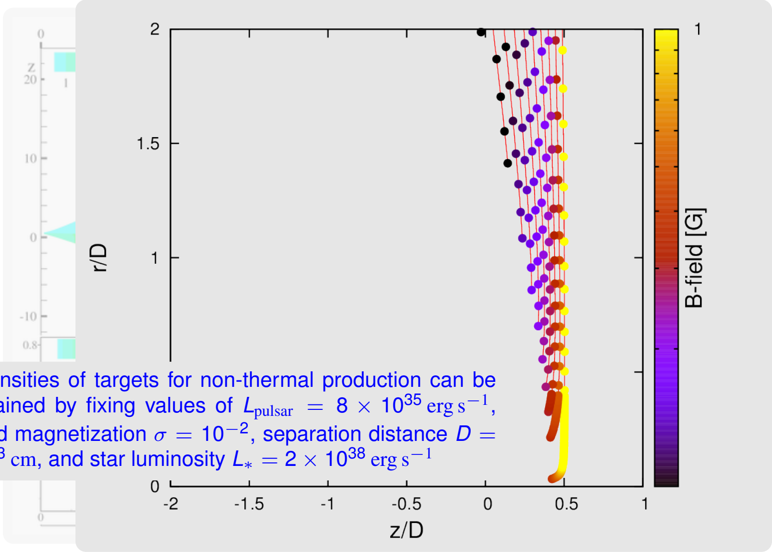

Intensities of targets for non-thermal production can be obtained by fixing values of $L_{\rm pulsar} = 8 \times 10^{35}\,{\rm erg\,s^{-1}}$, wind magnetization $\sigma = 10^{-2}$, separation distance $D = 10^{13}\,{\rm cm}$, and star luminosity $L_* = 2 \times 10^{38}\,{\rm erg\,s^{-1}}$

Hydrodynamic Solution:$\eta = 1$

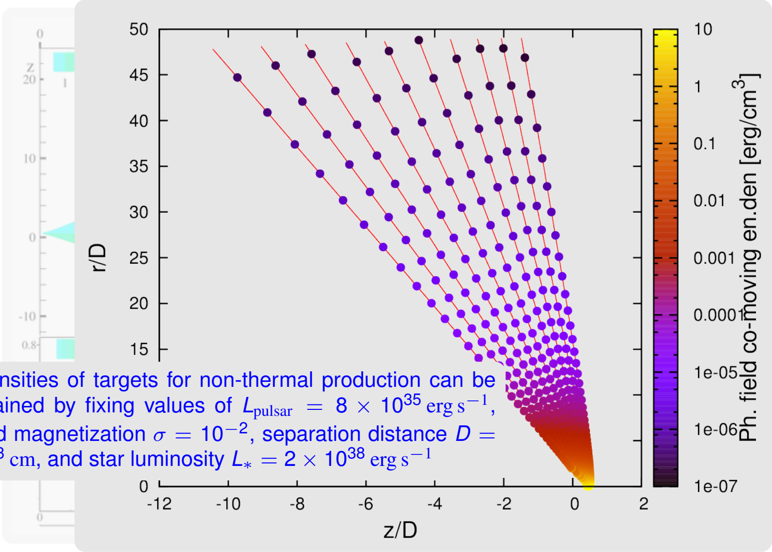

Intensities of targets for non-thermal production can be obtained by fixing values of $L_{\rm pulsar} = 8 \times 10^{35}\,{\rm erg\,s^{-1}}$, wind magnetization $\sigma = 10^{-2}$, separation distance $D = 10^{13}\,{\rm cm}$, and star luminosity $L_* = 2 \times 10^{38}\,{\rm erg\,s^{-1}}$

Hydrodynamic Solution: $\eta = 1$

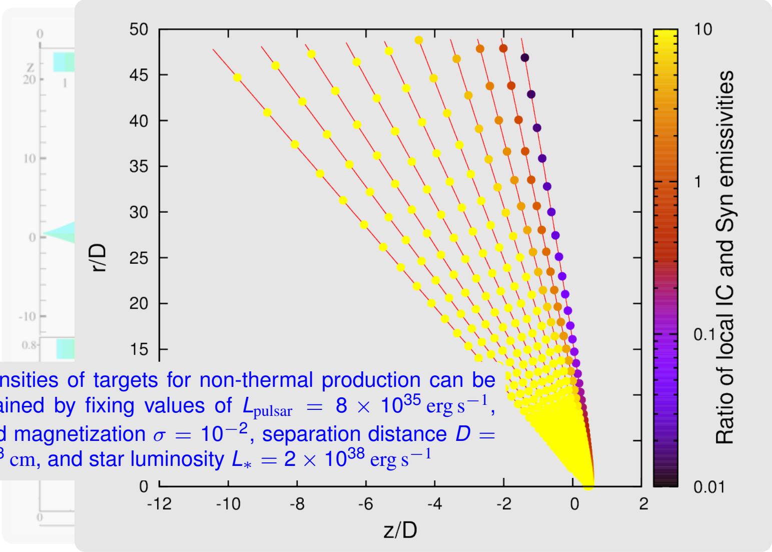

Intensities of targets for non-thermal production can be obtained by fixing values of $L_{\rm pulsar} = 8 \times 10^{35}\,{\rm erg\,s^{-1}}$, wind magnetization $\sigma = 10^{-2}$, separation distance $D = 10^{13}\,{\rm cm}$, and star luminosity $L_{*} = 2 \times 10^{38}\,{\rm erg\,s^{-1}}$

Hydrodynamic Solution: $\eta = 1$

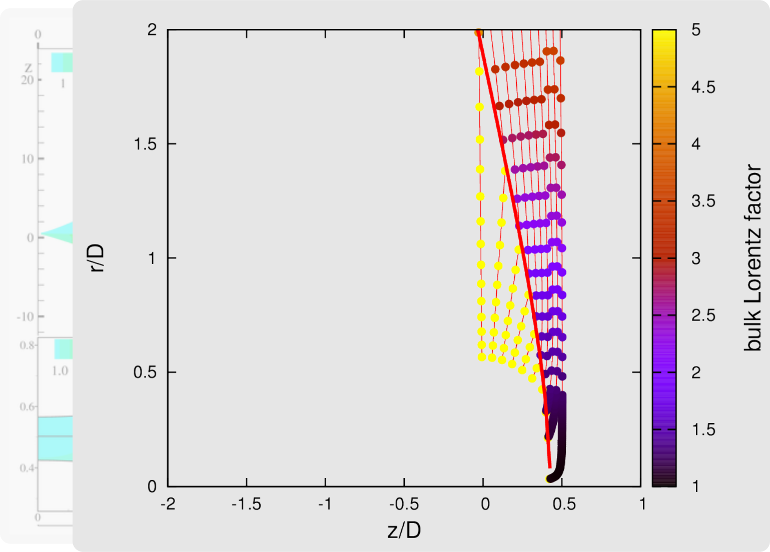

Summary

- It is likely that a relativistic outflows are produced at interaction of stellar-pulsar winds
- Relativistic boosting works in a very unusual way in these systems
- Different HD effect appear to have a strong influence on intensity of the emission